



Trade Science Inc.

# Materials Science

*An Indian Journal*


---

**Full Paper**

MSAIJ, 4(4), 2008 [237-244]

## Catalytic evaluation of sulfated zirconia pillared clay in n-hexane transformation

D.Radwan<sup>1\*</sup>, L.Saad<sup>1</sup>, S.Mikhail<sup>1</sup>, S.A.Selim<sup>2</sup><sup>1</sup>Egyptian Petroleum Research Institute, Refining Division, Hai Elzohoor, Nasr City, Cairo-1172, (EGYPT)<sup>2</sup>Ain Shams University, Faculty of Science, El-Abasia, Cairo-1172, (EGYPT)

Fax: +2022747433

E-mail: lamiakaid@yahoo.com

Received: 20<sup>th</sup> April, 2008 ; Accepted: 25<sup>th</sup> April, 2008

### ABSTRACT

Sulfated zirconia pillared clay (SZ-PILC) was prepared by adding sulfates to zirconium species before the pillaring process. The intercalated clay was then characterized by DTA, FTIR, X-ray diffraction and N<sub>2</sub>-adsorption techniques. It was found that, pillaring process using sulfated zirconia as intercalating agent gave rise to good thermal stability, significant increase in the main d-spacing values characterizing the bentonite clay from 12 Å to 15, 17 and 19 Å, and created dominant microporosity feature. The catalytic conversion of n-hexane was examined by both sulfated zirconia catalyst and sulfated zirconia pillared clay, using a flow system operating under atmospheric pressure and at reaction temperature range 180-300°C. Results indicated that, SZ-PILC is more active than sulfated zirconia (SZ) catalyst in n-hexane transformation. The major primary reaction was isomerization, giving monobranched and dibranched isomers. Small amounts of cracked, cyclic and aromatic products were also observed.

© 2008 Trade Science Inc. - INDIA

### KEYWORDS

Pillared clay;  
Sulfated zirconia;  
Catalytic activity.

### 1. INTRODUCTION

In order to protect the environment, several sets of regulations have been established. Owing to this legislation, great interest has been devoted to the substitution of unfriendly and corrosive liquids, used in chemical and petrochemical industries by solid catalysts. On this basis, clays may constitute very promising substitutes.

When inorganic species are introduced into the interlayers of the clay, the resulting nanocomposite can be used as a catalyst for specific reactions. The inter-

calated species are able to prevent the collapse of the interlayer spaces giving rise to two-dimensional porous materials "pillared clay materials"<sup>[1,2]</sup>.

The pillared clays are usually used as cracking catalysts because they develop a good acidity and good thermal stability. Beside the acidity of the clay layers, the metal oxide pillars also show an acidic character. However, the modification of the metal oxide pillars by electronegative ions like sulfates, results in the production of strongly acid components<sup>[3,4]</sup>, where the inductive effect of the S=O group increases the charge in the neighbor metal cation (M<sup>+</sup>).

## Full Paper

Faran-Torres and Grange and others modified the acidity of  $ZrOCl_2$  montmorillonite by adding  $(NH_4)_2SO_4$  during the intercalation reaction<sup>[5-9]</sup>. The intercalation of zirconium sulfate hydroxyl complex in Na-montmorillonite using zirconium acetate as a precursor was also studied<sup>[10]</sup>.

In the present investigation, the effect of sulfate precursors on the textural properties and catalytic activity of the prepared sulfated zirconia pillared clay catalysts is studied.

## 2. EXPERIMENTAL

### 2.1 Preparation method

#### 2.1.1. Preparation of sulfated zirconia (SZ) catalyst

Ammonium sulfate was added to 0.1 mole  $ZrOCl_2$  solution freshly prepared with  $SO_4:Zr$  molar ratio equal to 0.15<sup>[9]</sup>. The solution was then subjected to reflux for 4h, then evaporated and dried at 120°C for 4h, followed by calcination at 450°C in the presence of purified air for 6h.

#### 2.1.2. Preparation of sulfated zirconia pillared clay (SZ-PILC)

The starting clay material (bentonite from Alexandria district) was dispersed in freshly prepared 1M solution of  $NH_4OH$  (10g/L) for 24 hours, and then aged in distilled water for at least three days. The suspended part then centrifuged, washed by distilled water, and dried at room temperature. The solid sample obtained was sieved to 200 meshes. The chemical analysis of this clay presented in TABLE 1.

The intercalated clay was prepared by adding the freshly refluxed sulfated zirconia solution drop wise to 10g/l clay suspension. The slurry was refluxed at 100°C for 4h, washed by distilled water and left to dry at room temperature<sup>[9]</sup>. The sample was then calcined in a flow of purified air at 450°C.

### 2.2. Characterization of the prepared pillared clay

The structure of the prepared interlayered clay

TABLE 1: Chemical analysis of the clay

SiO <sub>2</sub>	Al <sub>2</sub> O <sub>3</sub>	FeO <sub>3</sub>	Na <sub>2</sub> O	MgO	K <sub>2</sub> O	IL*
56.91	16.95	6.53	5.85	0.87	1.32	11.55

\*Ignition loss is determined by burning one gram sample at 1000°C till constant weight.

samples was studied by various techniques;

Differential thermal analyses (DTA) were carried out in temperature range from room temperature to 1000°C on the prepared catalyst samples under a flow of Ar using SETARAM Labsys TG-DSC16 to trace the structure changes accompanying the thermal treatment.

Infrared spectroscopic analysis (FTIR) was carried out using ATI Matt son 1001 in the IR region of 400-4000 $cm^{-1}$ , to characterize the main constituents of the prepared samples. All samples were grinding with potassium bromide (KBr) powder and then pressed into a disk before analysis.

X-Ray diffraction analyses (XRD) were carried out by a Shimadzu XD-1 diffractometer using Cu-target Ni-filtered to study the different phases accompanied the intercalation process.

The textural properties were determined from the adsorption-desorption isotherms measured at liquid nitrogen temperature using NOVA 3200e sorption, the specific surface area was evaluated by the BET method, pore size and pore volume data were obtained by the BJH method. All samples were degassed at 200°C for 17h in nitrogen atmosphere prior to adsorption.

### 2.3. Catalytic activity

Catalytic transformation of n-hexane over the prepared pillared interlayer clay catalysts was performed in a flow system operated under atmospheric pressure, at the temperature range 180-300°C, hydrogen flow rate 35ml/min, catalyst volume 5ml and liquid hourly space velocity (LHSV) 0.6  $hr^{-1}$ .

The product analysis was performed using Perkin-Elmer gas chromatograph with hydrogen flame ionization detector; capillary column was used to analyze the reaction products throughout this investigation.

## 3. RESULTS AND DISCUSSION

### 3.1 Structural characterization

#### 3.1.1 Thermal analysis

Figure 1(a-c) illustrates the differential thermal analysis (DTA) profiles for SZ sample, parent bentonite clay, and the prepared SZ-PILC.

DTA profile for SZ (Figure 1a) catalyst exhibits four endothermic features. Three endotherms occur below

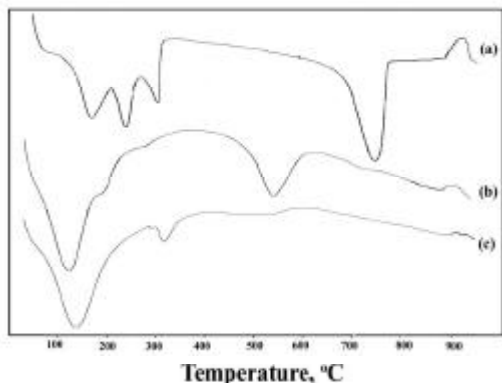


Figure 1 : Differential thermal profiles for; a-Sulfated zirconia, b- Parent bentonite clay, c-SZ-PILC (dried)

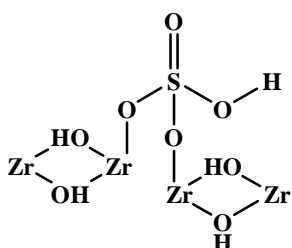


Figure 2 : Sulfated zirconia structure<sup>[17]</sup>

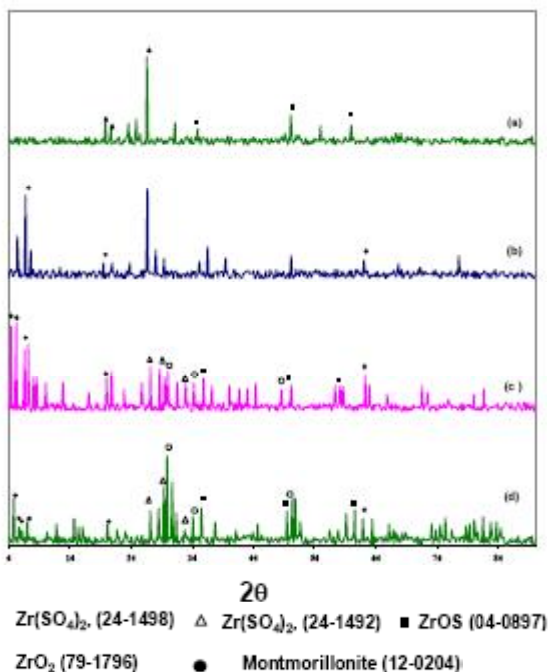


Figure 3: XRD pattern for; a-Sulfated zirconia, b- Raw clay, c-SZ-PILC (dried) d- SZ-PILC (calc. 450°C)

TABLE 2 : Textural properties of the prepared samples

Sample	$S_{BET}$ , $m^2/g$	$V_p$ , cc/g	Pore width, Å
Parent clay	71.188	0.225	63.43
SZ-PILC (calc. 450°C)	78	0.08	22.28

400°C that can be identified as,

At  $\approx 110^\circ\text{C}$ : evolution of water molecules loosely adsorbed on the external surface, At  $\approx 200^\circ\text{C}$ : evolution of water molecules strongly associated with hydroxyl zirconium cations<sup>[11]</sup> and At  $\approx 300^\circ\text{C}$ : dehydroxylation and crystallization of bulk  $\text{Zr}(\text{OH})_4$  into tetragonal  $\text{ZrO}_2$  [V.Parvulescu, S.coman, P.Gränge, V.I.Parvulescu: Applied catalysis, 176, 27-43 (1999). The fourth endothermic feature at  $\approx 700^\circ\text{C}$  is attributed to the loss of  $\text{SO}_2$ <sup>[12]</sup>. One exothermic peak at  $\approx 900^\circ\text{C}$  is due to phase transformation of  $\text{ZrO}_2$  from metastable tetragonal phase to stable monoclinic phase<sup>[13]</sup>.

The DTA curve for the starting bentonite clay shows three main endothermic processes, the endotherm at  $\approx 100^\circ\text{C}$  corresponds to the loss of physically adsorbed water on the external surface, and the presence of shoulder near to  $200^\circ\text{C}$  indicates that this raw material is calcium-montmorillonite type<sup>[14]</sup>. Very small endothermic feature at  $\approx 280^\circ\text{C}$  referred to escape of interlayer water. Higher temperature endotherm at  $\approx 550^\circ\text{C}$  corresponds to the beginning of the interlayer collapse as a result of the decomposition of the silicate structure with loss of a water molecule per formula unit by dehydroxylation<sup>[15]</sup>. The exothermic peak that appears at  $930^\circ\text{C}$  is a structural one, which attributed to the destruction of montmorillonite and formation of new phase.

The DTA profile for the prepared SZ-PILC exhibits three endotherms in the range  $100\text{--}300^\circ\text{C}$ , the first one results from the loss of water, is broader than that for the parent clay due to strong solvation power of Zr-cationic species. Meanwhile, the second endotherm at  $300^\circ\text{C}$  can be attributed to the dehydroxylation of bulk  $\text{Zr}(\text{OH})_4$  to  $\text{ZrO}_4$  or the substitution of terminal Zr-OH group by  $\text{SO}_4^{2-}$ <sup>[16]</sup> to form sulfated zirconia structure (Figure 2).

It is worth noting that, the observed diminish of the endothermic feature at  $\approx 550^\circ\text{C}$  (the dehydroxylation of the silicate structure) may attributed to the cross linking of sulfated zirconia intercalated species into the interlayer hydroxyl group keeping the layer apart thereby preventing its collapse.

### 3.1.2 X-ray Analysis

X-ray diffraction patterns of all investigated samples; sulfated zirconia (SZ), bentonite clay, dried SZ-PILC and SZ-PILC respectively, are illustrated in figure 3(a-

## Full Paper

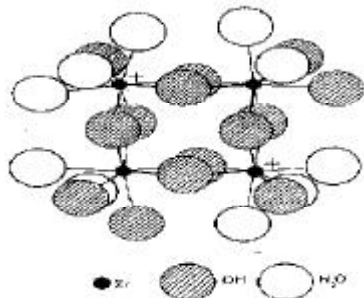


Figure 4 : Probable form of the  $[\text{Zr}(\text{OH})_{14}(\text{H}_2\text{O})_{10}]_2^+$  complex<sup>[18]</sup>

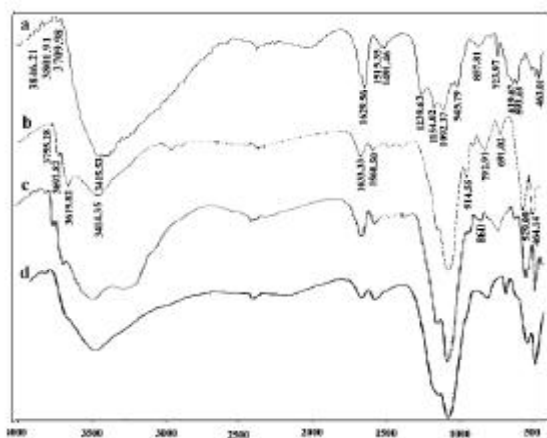


Figure 5: IR spectrum for; a-sulfated zirconia, b-Parent clay, c-SZ-PILC (dried), d-SZ-PILC (calc. 450°C).

d) and presented in TABLE 2.

The diffractogram for SZ (Figure 3a) reveals highly crystalline phase corresponds to zirconium sulfate (ASTM 24-1498), in addition to, the main characteristic lines for ZrOS (ASTM 04-0897).

The diffraction pattern for the parent clay (Figure 3-b) exhibits the main d-spacing identifying montmorillonite at: 12.99, 4.53 and 1.49 Å (ASTM 12-0204), with some basal reflections for kaolinite mineral at d-values near, 7.2 and 3.33 Å, in addition to quartz at, 3.36, 3.49 Å together with traces of feldspars.

For dried SZ-PILC (Figure 3c), the pattern reveals new basal reflections [15.28, 16.75, and 19.97 Å] at  $2\theta$  lower than 7, in addition to, the main basal reflections for montmorillonite which may indicates the penetration of the sulfated polycationic zirconia species into the interlamellar region, probing apart the interlayer structure and resulting in an observed expansion in the interlayer distance. However, the creation of various high d-values (Figure 3c) at  $2\theta < 7$  may be attributed to the orientation of the polycationic zirconium species in

the inter layer region, either as a double layer of flat-lying complexes (Figure 4), or as a single layer of complexes standing normal to the interlayer region is reasonably taking into account as stated by S. Yamanaka and W. Brindley<sup>[17]</sup>.

Furthermore, the pattern (Figure 3-c) exhibits also different characteristic lines for  $\text{Zr}(\text{SO}_4)_2$  [ASTM 24-1492 and ASTM 24-1498] which may indicates the existence of isolated and poly-nucleated sulfated species, in addition to, the main lines for ZrOS [ASTM 04-0897] and the basal reflection for tetragonal zirconia [ASTM 79-1796].

The diffractogram for calcined SZ-PILC (figure 3-d) indicates little compaction in the interlayer spacing to  $\approx 17.9 \text{ \AA}$  instead of  $19.97 \text{ \AA}$ , may be due to the partial removal of the interlayer coordinated water upon heating at  $450^\circ\text{C}$ . An increase in the line intensities corresponding to  $\text{Zr}(\text{SO}_4)_2$ , ZrOS and  $\text{ZrO}_2$ , (due to the decomposition of the poly-nucleated intercalated species) are also observed.

### 3.1.3 FTIR spectroscopy

Figure 5 (a-d) shows representative IR spectra for SZ, parent bentonitic clay, SZ-PILC and SZ-PILC respectively.

The spectrum for the prepared SZ (Figure 5-a) catalyst shows two types of isolated Zr-OH groups that are in the fundamental OH stretching region located in the range  $3846\text{--}3710\text{ cm}^{-1}$ . However, the OH bands between  $3800\text{--}3700\text{ cm}^{-1}$  are actually assigned to the terminal OH group<sup>[18]</sup>. The spectrum exhibits also a broad band between  $3600\text{--}2850\text{ cm}^{-1}$  with a maximum centered at  $3415\text{ cm}^{-1}$  which is attributed to acidic OH groups. Furthermore, characteristic sulfate bands at  $1515$  and  $1490\text{ cm}^{-1}$  are assigned to asymmetric and symmetric stretching modes of sulfate groups bound via two oxygen atoms to the zirconium ion. Bands at  $1092$ ,  $1154$  and  $1239\text{ cm}^{-1}$  are assigned to asymmetric and symmetric stretching modes of oxygen bound to the sulfur of sulfate<sup>[19]</sup>.

However, the mechanism of formation of covalent sulfates and poly sulfates allow us to ascribe<sup>[20]</sup>;

- The bands concentrated at  $\nu < 1400\text{ cm}^{-1}$  to isolated surface  $\text{SO}_4^{2-}$  groups and are postulated to be bonded to the oxide network by more than two S-O-Zr bridges<sup>[19]</sup>.

- The bands at  $\nu' \geq 1400 \text{ cm}^{-1}$  to poly-nuclear surface sulfates probably of the type pyrosulfates  $[\text{S}_2\text{O}_7]$ .
- Stretching band located at  $\nu' \geq 1350 \text{ cm}^{-1}$  are ascribed to highly covalent sulfates ( $\nu'_{\text{S-O}}$ ).
- Several low frequency bands at  $\nu' \leq 1150 \text{ cm}^{-1}$  are due to ( $\nu'_{\text{S-O}}$ ) stretching modes<sup>[21,22]</sup>.

The spectrum for bentonite clay (figure 5-b) reveals a large and relatively broad absorption band at OH-stretching region ranging from 3750-3400  $\text{cm}^{-1}$  giving rise to three clear peaks at 3692, 3619 and 3414  $\text{cm}^{-1}$  that can be assigned to the bonded and unbounded OH of the clay mineral. The absorption band at  $\approx 3692 \text{ cm}^{-1}$  is ascribed to those hydroxyl groups constituting one side of the sheet, some times referred to as inner surface hydroxyls<sup>[23]</sup>. The absorption band at 3619  $\text{cm}^{-1}$  is assigned to hydroxyl groups located inside the sheet being situated at the middle layer between the tetrahedral and octahedral that constitute the bentonitic structure<sup>[24]</sup>. The large broad band centered at  $\approx 3415 \text{ cm}^{-1}$  is characterized for the vibration frequencies of OH groups on the clay surface and/or on the inside of the silicate sheet structure.

The band centered at 1630  $\text{cm}^{-1}$  is assigned to the OH vibration of the interlayer molecular water whereas, the strong band at the range 1150-920  $\text{cm}^{-1}$  is believed to characterize bentonite being related to the OH-Al group.

Several minor absorption bands in the range of 690-920  $\text{cm}^{-1}$  may be ascribed to the (Si-O) group of kaolinite and bentonite minerals. The two bands at the lower vibration region in the range 460-530  $\text{cm}^{-1}$  may correspond to the vibration of Si-O groups and Si-O-Al group of kaolinite respectively.

Furthermore, the spectrum of dried SZ-PILC (figure 5-c) displays the main constituent bands of bentonite clay, in addition to the appearance of relatively sharp band at  $\approx 1398 \text{ cm}^{-1}$  that is attributed to a highly covalent and/or poly-nuclear sulfate species (2) intercalated into the inter-lamellar region of the clay. Meanwhile, the small broad band at  $\approx 1550 \text{ cm}^{-1}$  may also be attributed to the existence of some isolated sulfate groups. However, an observed broadening in the OH-stretching band at  $\approx 3600\text{-}3000 \text{ cm}^{-1}$  might be attributed to either the partial substitution of some OH groups of the interlayer structure by  $\text{SO}_4^{2-}$  groups or the cross-

linking of sulfated polycationic species to the OH groups constituting the silica-silica tetrahedral sheets of bentonite.

The spectrum of calcined SZ-PILC exhibits generally; relative broadening of most bands ascribed to the bentonite structure 1043, 1110 and 3700-3400  $\text{cm}^{-1}$  as well as the disappearance of the characteristic band for polynucleated sulfate species at 1398  $\text{cm}^{-1}$ . This behavior can be referred to the slight compaction in the inter layer spacing accompany the partial removal of the interlayer water [broadening of the band at 1630  $\text{cm}^{-1}$ ] as well as the probable decomposition of poly-nucleated sulfated species to smaller sulfated zirconium species.

### 3.1.4 Textural characteristics

Surface properties for the prepared materials were determined from nitrogen adsorption isotherms conducted at -196°C.

The data obtained including, specific surface area ( $S_{\text{BET}}$ ), total pore volume (Vp), and mean pore radius ( $r_{\text{H}}$ ) are presented in TABLE 2.

The adsorption isotherms represented in figure 6-I belong to type IV of Brunauer classification<sup>[25]</sup> and exhibited  $\text{H}_2$  hysteresis loop (according to IUPAC classification), closing at  $P/P^0 \sim 0.4$  denoting the presence of aggregate of plate like particles giving rise to slit-shaped pore<sup>[26]</sup>.

The  $S_{\text{BET}}$  values of studied materials computed from linear plots of the  $S_{\text{BET}}$  equation revealed an observed increase in surface area of the parent clay from (71  $\text{m}^2/\text{g}$ ) to (78  $\text{m}^2/\text{g}$ ) for the pillared one, meanwhile, the total pore volume and average pore radius decreased significantly.

The noticeable increase in the surface area of the calcined sulfated zirconia pillared clay are most probably arise from the creation of microporosity feature through the dispersion of smaller zirconia species (pillars) in the interlamellar region. However, the decrease in either total pore volume or average pore radius may indicate the migration of some zirconia species into the interlamella pores and their occupation to a portion of them.

The porous structure of the prepared materials was also identified by t-method of de Boer et al., (J.H. De Boer, B.G. Linen, T.J. Osniga, Metallurgia 4, (1965) 319). V-t plot for the parent clay which lead to straight



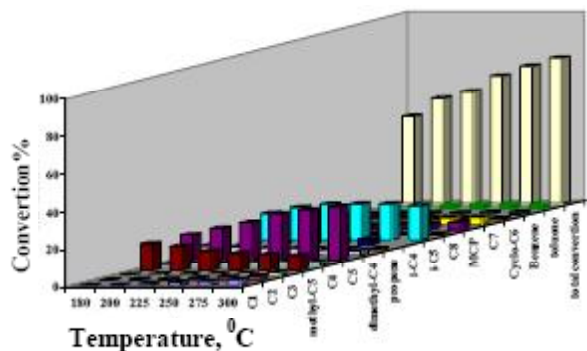


Figure 9 : Product distribution of n-hexane conversion over SZ-PILC catalyst

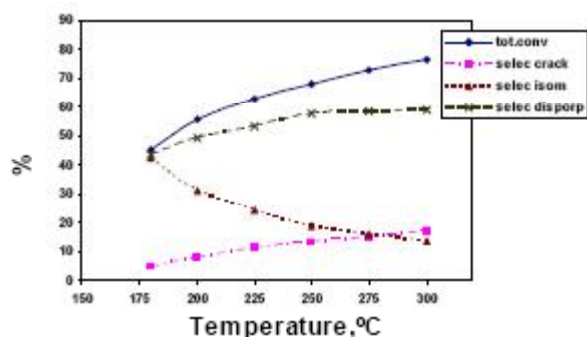
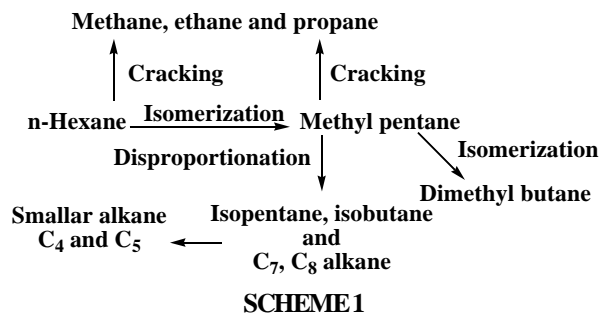


Figure 10 : Effect of temperature on the selectivity of SZ-PILC towered n-hexane converted products



reaction at temperatures varying between 180-300°C. Data are illustrated in Figures 7-10.

The data indicates the typical dependence of n-hexane conversion on the reaction temperature over both catalysts, thus, total conversion increases with raising the reaction temperature (Figure 7).

On SZ catalyst the product distribution of n-hexane conversion revealed that methyl-pentane (iso-hexane) is the major isomeric product, its selectivity decreases gradually with the increase in the total conversion (figure 8).

On the other hand iso-butane is considered as the predominant product at all reaction temperatures, its

selectivity increases with the total conversion. Considerable amount of isopentane is also obtained with incremental selectivity with the increase in the total conversion (figure 8). Propane, ethane and methane were within detection limits. Skeletal isomers (i-C7 and i-C8) were among the minor products with selectivity  $\leq 5\%$  at the highest total conversion.

Conversion of n-hexane over calcined SZ-PILC seemed to follow the same trend as SZ. Product distribution of n-hexane conversion over SZ-PILC (Figure 9) revealed two isomeric products for n-hexane, mono-branched isomer (methyl pentane) and dibranched isomer (dimethyl butane) that decreased with the increase in reaction temperature. Their selectivity exhibited a gradual decrease with the increase in the total conversion (Figure 10). The sharp decrease of these isomeric products at reaction temperatures over 200°C is most probably resulted from the consecutive cracking reactions and is accompanied by a marked increase in the yield of iso-pentane and iso-butane.

Moreover, the significant increase in C<sub>6</sub><sup>+</sup> products (C<sub>7</sub> and C<sub>8</sub>) with the total conversion may be resulted from disproportionation reaction<sup>[28,29]</sup>. Methylcyclopentane, cyclohexane, benzene and toluene are also formed. The formation of these cyclic products may take place via either a selective or a non-selective dehydrocyclization process of n-hexane and corresponded to the reverse reaction of a selective or non-selective cyclic mechanism<sup>[30,31]</sup>. Furthermore, cyclohexane may undergo dehydrogenation leading to the production of benzene and 1-5 ring contraction that giving rise to methyl cyclopentane<sup>[32]</sup>.

From the previous exploration for the products of n-hexane transformation over the investigated SZ-PILC, the reaction network in SCHEME1 can be suggested.

The reactions shown in the SCHEME are generally believed to proceed via carbenium ion mechanism<sup>[38]</sup>; however, the high abundance of iso-pentane and iso-butane may indicate the high preference of bimolecular reactions<sup>[33-35]</sup>. One of the possible routes would involve splitting at the center of n-hexane molecule to give a surface C<sub>3</sub> entity. This may not desorb as propane but seems to react with another C<sub>6</sub> unit to form a C<sub>9</sub> intermediate that produces iso-pentane and iso-butane<sup>[36,37]</sup>.

Consistent with this pattern, one would speculate

## Full Paper

the isomerization process to proceed via monomolecular mechanism that predominates initially followed by bimolecular mechanism that attributed to result in disproportionation processes.

### 4. CONCLUSION

The results presented in this work show that sulfated zirconium modified pillared clay can be obtained with good thermal stability, modified structural and textural properties. The results also indicated that SZ-PILC shows inferior performance in n-hexane transformation via isomerization, disproportionation and cracking reactions. The n-hexane isomerization takes place predominantly at the lower temperatures, whereas, disproportionation becomes predominant at the higher temperatures. The higher isomerization activity and selectivity of the modified sulfated zirconia pillared clay at lower temperatures, may inferred to acidity enhancement by the effect of sulfate groups. SZ-PILC catalyst is also active for the formation of dibranched product under the present experimental conditions, which implies that they can meet the demanding criteria for production of higher octane number alkanes.

### REFERENCES

- [1] D.E.W.Vaughan; *Catal.Today*, **2**, 187 (1988).
- [2] J.F.Lambert, G.Poncelet; *Top.Catal.*, **4**, 43 (1997).
- [3] N.Bouchenafa-saib, R Issaadi, P.Gränge; *Applied Catalysis*, **259**, 9-15 (2004).
- [4] R.Issaadi, F.O.Garin et al; *Catalysis Today*, **113**, 166-173 (2006).
- [5] E.M.Faran Torres, P.Gränge; *C.R.Acad.Sci.Belg.*, **4/5**, 113 (1990).
- [6] E.M.Faran Torres, P.Gränge; *Catal.Sci.Technol.*, **1**, 103 (1991).
- [7] E.M.Faran-Torres, E.Sham, P.Grang; *Catal.Today*, **15**, 515 (1992).
- [8] M.Katoh, H.Fujisawa, T.Yamaguchi; *Stud.Surf.Sci.Catal.*, **90**, 263 (1994).
- [9] S.Ben Chaabene, L.Bergaoui, A.Ghorbel, J.F.Lambert; *Stud.Surf.Sci.Catal.*, **143**, 1053 (2002).
- [10] L.Bergaoui, A.Ghorbel; *J.F.Lambert, Stud.Surf.Sci.Catal.*, **142**, 903 (2002).
- [11] C.R.Vera; *Appl.Catal.A:General*, **230**, 137-151 (2002).
- [12] R.Srinivasan et al.; *Applied Catalysis*, **130**, 135-155 (1995).
- [13] R.Srinivasan, T.Watkins, C.Hubbard, B.H.Davis; *Chem.Mater.*, **7**, 725 (1995).
- [14] I.Barshad; *Am.Miner.*, **35**, 225 (1950).
- [15] S.Yamanaka, G.W.Brindley; *Clay and Clay Minerals*, **27**, 119 (1979).
- [16] L.Binghui, R.D.Gonzalez; *Ind.Eng.Chem.Res.*, **35**, 3141 (1996).
- [17] S.Yamanaka, W.Brindley; *Clay and Clay Mineral*, **27**, 119 (1979).
- [18] W.Hertl; *Langmuir*, **5**, 96 (1988).
- [19] M.Bensitel, O.Saur, J.C.Lavalley, B.A.Morrow; *Mater.Chem.Phys.*, **19**, 147 (1988).
- [20] L.JBellamy; 'The Infrared of Complex Molecules', Chapman and Hall, London, (1987).
- [21] K.Nakamoto, 'Infrared and Raman Spectra of inorganic and Coordination Compounds', Wiley-Interscience, New York, 249 (1986).
- [22] N.B.Colthup, L.H.Daly, S.E.Wiberley; 'Introduction to Infrared and Raman Spectroscopy', Academic Press, New York, 353 (1975).
- [23] M.L.Ocelli, J.E.Lester; *Ind.Eng.Chem.Prod.Res.Dev.*, **24**, 27 (1985).
- [24] N.Lahav, U.Shani, J.Shabtai; *Clays and Clay Mineral*, **26**, 107 (1978).
- [25] K.S.W.Sing, D.H.Everett, R.A.W.Haul, L.Moscou, R.A.Pierotti, J.Rouquerol, T.Siemieniewska; *Pure Appl.Chem.*, **57**, 603 (1985).
- [26] A.Lecloux, J.P.Pirared; *J.Colloid Interface Sci.*, **70**, 265 (1979).
- [27] V.Parvulescu, S.Coman, P.Gränge, V.I.Parvulescu; *Apple.Catal.A.*, **27**, 176 (1999).
- [28] T.K.Cheung, B.C.A.Gates; *J.Catal.*, **168**, 522 (1997).
- [29] Regui, B.C.Gates; *Catal.Lett.*, **37**, 5 (1996).
- [30] Z.Paal; *Adv.Catal.*, **29**, 273 (1980).
- [31] F.G.Gault; *Adv.Catal.*, **30**, 267 (1982).
- [32] F.Garin, G.Maire; *Acc.Chem.Res.*, **22**, 100 (1989).
- [33] F.Garin, Andriamasinoro, A.Abdulamad, Sommer; *J.Catal.*, **131**, 199 (1991).
- [34] E.Iglesia, S.L.Soled, G.M.Kramer; *J.Catal.*, **144**, 238 (1993).
- [35] A.Sayari, Y.Yang, X.Song; *J.Catal.*, **167**, 346 (1997).
- [36] W.O.Haag, R.M.Dessau; *Proceedings of the 8<sup>th</sup> International Congress on Catalysis, Berlin (West)*, Verlag Chemie, Weinheim, **2**, 305 (1984).
- [37] N.Bouchenafa-Saib, R.Issaadi, P.Gränge; *Applied Catalysis*, **9**, 259 (2004).
- [38] S.G.Ryu, B.C.Gates; *Ind.Eng.Chem.Res.*, **37**, 786 (1998).